A Comparison of Passive Microwave Emission Models for Estimating Brightness Temperature at L- and P-band Under Bare and Vegetated Soil Conditions

Foad Brakhasi, Jeffrey P. Walker, Jasmeet Judge, Pang-Wei Liu, Xiaoji Shen, Nan Ye, Xiaoling Wu, In-Young Yeo, Nithyapriya Boopathi, Edward Kim, Yann Kerr, and Thomas Jackson

***Abstract*— P-band radiometry has been demonstrated to have a deeper sensing depth than at L-band, making the consideration of multi-layer microwave interactions necessary. Additionally, the scattering and phase interference effects are different at P-band, requiring a re-consideration of the need for coherent models. However, the impact remains to be clarified, and understanding the validity and limitations of these models at both L-band and P-band is crucial for their refinement and application. Therefore, two general categories of microwave emission models, including two stratified coherent models (Njoku and Wilhite) and four incoherent models (conventional tau-omega model and three multi-layer models being zero-order, first-order, and incoherent solution), were intercompared for the first time on the same dataset. This evaluation utilized observations of L-band and P-band radiometry under different land cover conditions from a tower-based experiment in Victoria, Australia. Model estimations of brightness temperature (TB) were consistent with measurements, with the lowest root mean square error (RMSE) at P-band V-polarization under corn (2 K) and the highest RMSE at L-band H-polarization under bare soil (13 K). Coherent models performed slightly better than incoherent models under bare soil (3 K less RMSE), while the opposite was true under vegetated soil conditions (1 K less RMSE). Coherent and incoherent models showed maximum differences (3 K at P-band, 2 K at L-band), correlating strongly with soil moisture variations at 0-10 cm. Findings suggest that coherent and incoherent models perform similarly; thus, incoherent models may be preferable for estimating TB at L- and P-band due to reduced computational complexity.**

***Index Terms*— Soil moisture profile, Coherent, Incoherent, P-band, L-band, Passive microwave.**

I. INTRODUCTION

Soil moisture constitutes only a small fraction of the global freshwater (0.05% out of 2.5%) but is a key factor for everything linked to life on Earth [1]. Excess soil moisture can lead to natural disasters such as floods and landslides [2], while a deficit in soil moisture can result in wildfires and drought [3, 4], which can have detrimental effects. Adequate soil moisture is also essential for plant growth, photosynthesis, and evapotranspiration, which supports food security and the environmental conditions necessary for human survival. While *in situ* measurements of soil moisture can be sufficiently accurate for specific applications, the high spatial and temporal variability of soil moisture makes this method impractical for use at larger scales. Due to the development of remote sensing technologies, it is now possible to obtain regular soil moisture products at a global scale, overcoming the limitations of *in situ* measurements. Although it has a higher spatial resolution, soil moisture retrieval utilizing active microwave systems is confounded by the effects of surface roughness and vegetation [5, 6], making passive microwave the preferred approach for many applications [7]. Consequently, the Soil Moisture and Ocean Salinity (SMOS; [8]) and Soil Moisture Active Passive (SMAP; [9]) missions by the European Space Agency (ESA) and National Aeronautics and Space Agency (NASA), launched in 2009 and 2015 respectively, have both utilized passive microwave technology. These have led to mature near-surface soil moisture products using L-band (~21 cm) radiometers.

L-band microwave remote sensing is only able to detect soil moisture down to around 5 cm below the surface, and is affected by vegetation and surface roughness, leading to a shallower sensing depth and degraded retrieval precision when compared to longer wavelengths [10]–[12] . However, a complete understanding of many environmental applications requires information on the moisture in deeper layers of the soil. Furthermore, having information of the actual distribution of soil moisture within the vadose zone can be important in managing effective irrigation, because the roots of major crops are located in this zone [13]. Therefore, it is desirable to retrieve the soil moisture at different depths rather than simply a single value that

This research was funded in part by the Australian Research Council under Discovery Grant DP170102373, and Linkage, Infrastructure, Equipment and Facility Grants LE0453434 and LE150100047. (Corresponding author: Foad Brakhasi.)

Foad Brakhasi, Jeffrey P. Walker, Nan Ye and Xiaoling Wu are with the Department of Civil Engineering, Monash University, Clayton, Australia (e-mails in order: foad.brakhasi@monash.edu, jeff.walker@monash.edu, nan.ye@monash.edu, xiaoling.wu@monash.edu).

Jasmeet Judge is with Department of Agricultural and Biological Engineering, University of Florida, Gainesville, USA (e-mail: jasmeet@ufl.edu).

Pang-Wei Liu and Edward Kim are with Hydrological Sciences Branch, NASA Goddard Space Flight Center, Greenbelt, USA (e-mails in order: pang-wei.liu@nasa.gov, edward.j.kim@nasa.gov).

Xiaoji Shen is with the National Key Laboratory of Water Disaster Prevention, and Yangtze Institute for Conservation and Development, Hohai University, Nanjing, China (e-mail: xiaoji.shen@hhu.edu.cn).

In-Young Yeo is with School of Engineering, The University of Newcastle, Callaghan, Australia (e-mail: in-young.yeo@newcastle.edu.au).

Nithyapriya Boopathi is with IITB-Monash Research Academy, Mumbai, India (e-mail: nithyapriya.boopathi@monash.edu).

Yann Kerr is with Centre d'Etudes Spatiales de la Biosphère, Toulouse, France (e-mail: yann.kerr@cesbio.cnes.fr).

Thomas Jackson is with USDA ARS Hydrology and Remote Sensing Laboratory (Retired), Beltsville, USA (e-mail: tjwater01@gmail.com).

represents the average for the soil profile. To address this need, remote sensing technologies operating at lower frequencies such as P-band (~40 cm wavelength) have been developed [14]. In addition to providing information about the moisture content distribution in a deeper layer of soil [15], microwave signals at P-band may be better suited for soil moisture retrieval under densely vegetated and topographically complex environments, due to its reduced sensitivity to vegetation [16] and surface roughness [11].

Radiative transfer models simulate the microwave signal's interactions and propagations within the soil, vegetation, and atmospheric mediums until they reach the sensor. The models structure involved in soil moisture, soil temperature, surface roughness, and/or vegetation water content retrievals is governed in two ways: by forward modeling or by inverse modeling. Consequently, the accuracy of the retrieved parameters of interest using either method depends heavily on the validity of the forward model [16, 17]. In accordance with the principles of microwave remote sensing theory, the proximity of high soil moisture to the surface exhibits a strong correlation with brightness temperature (TB). This correlation is attributed to the influence of soil dielectric constant on soil microwave emissivity, consequently impacting TB. Studies have demonstrated the advantage of assimilating TB over soil moisture into a land surface model, with improved predictions of soil moisture and soil temperature [18, 19]. Accordingly, assimilation can improve both the retrieval of vertical soil moisture profile information [21] and horizontal resolution [22].

Forward radio transfer modelling plays a major role in land data assimilation systems by acting as an observation operator to provide a link between the forecast model states (i.e., soil moisture and temperature) and the observational variable (i.e., TB). The calculated TB is affected by uncertainties in the model states and can thus introduce biases. Hence, the performance of radiative transfer models can largely determine the capability of assimilation systems in accurately simulating the surface states. Successfully using the satellite TB observations therefore requires an unbiased and accurate [23], calibrated [23, 24] model of microwave radiative transfer processes, affecting the innovations (difference between TB observations and radiative transfer model TB simulations) used to update the soil moisture analysis states. Therefore, as the uncertainties in the assimilated observations decrease, the precision of the analysis improves [26]. Consequently, the validity of radiative transfer models, whether used to retrieve soil moisture directly from TB observations or within a data assimilation framework, is essential.

There are two main types of radiative transfer models used to simulate brightness temperature, called coherent and incoherent models. Coherent models calculate the emission by tracking the phase of the electric field and coupling the emissivity of the surface layers to deeper layers. In contrast, incoherent models calculate the intensity of radiation directly at the air-soil interface by assuming a homogeneous medium [27]. The main difference between the predictions of the two models lies in the effects of wave interference, the frequency employed, and the steepness of the soil moisture gradient near the surface. Accordingly, the derived coherent and incoherent emissivity's have the same general trend, but the coherent emissivity also exhibits phase-interference oscillations [18]. Incoherent models are computationally and mathematically simpler than coherent models, but their accuracy is expected to be lower, particularly at longer wavelengths [27]. Moreover, the accuracy of incoherent models compared to coherent models at P-band is unknown as this comparison has never been made. Additionally, with the emergence of P-band technology, it has been demonstrated that a deeper sensing depth can be achieved [10], making the consideration of multi-layer microwave interactions necessary.

Multi-layer models have not been extensively utilized to date because L-band and higher frequencies have shallow sensing depths. However, with the different scattering/interference effects at P-band, a re-consideration of coherent model use is required. Therefore, this study aimed to fill this gap by conducting a detailed comparison of coherent and incoherent emission models at both L-band and P-band on the same dataset, providing clarity for the remote sensing community on the usefulness of coherent models over incoherent models, along with a comparison of multi-layer and conventional incoherent models. Beyond a mere comparative analysis, the objective was to contribute to the future improvement of forward modeling and soil moisture inversion for satellite-based observations. By leveraging observations from an extensive tower-based experiment, not only could the strengths and limitations of existing models be identified, but also enhancements and refinements could be proposed. Moreover, this study aligns with a broader objective of advancing soil moisture modeling from satellite observations, offering insights that can inform the design and implementation of future missions operating at P-band radiometry.

II. Data

An experiment with tower-based radiometers was conducted at Cora Lynn, Victoria, Australia, comprising a comprehensive setup as shown in Fig. 1. The tower was situated at the center of a paddock measuring 150 m × 150 m in size and divided into four quadrants. Each quadrant was managed with different land conditions, including vegetation (bare, grass, wheat, and corn) and surface roughness (smooth, random, and furrow). The tower carried two radiometers, being the Polarimetric P-band Multi-beam Radiometer (PPMR) and the Polarimetric L-band Multi-beam Radiometer (PLMR), which were rotated and tilted to capture the four quadrants at different incidence angles. In this study, L-band and P-band observations at an incidence angle of approximately 40° were used. Four soil moisture and temperature stations were set up, with one on the border of each quadrant, to simultaneously measure soil moisture and temperature profiles from the surface to a depth of 60 cm in increments of 5 cm. The average soil texture of the site is 18.3% clay (18%, 17%, 17% at depths of 5 cm, 20 cm, and 50 cm, respectively), 13.7% sand (12%, 11%, 20% at depths of 5 cm, 20 cm, and 50 cm, respectively), and 68% silt (71%, 69%, 62% at depths of 5 cm, 20 cm, and 50 cm, respectively), indicating a silty loam soil. This research examined six periods of data,

which included three periods of bare soil (April 2019, March 2020, December 2020), a period of grass (March 2018), a period of wheat (December 2018), and a period of corn (December 2020 to February 2021), as depicted in Fig. 3 and Fig. 4.

This study employed an extensive collection of data measured from quadrant 2 and station 126 at 6 AM/PM, consisting of 141 days with simultaneous TB observations at an incidence angle of 40°, using both L-band and P-band frequencies, along with supplementary data. These ancillary data included measurements of vegetation water content (VWC), encompassing the water content of the entire plant, including stems, leaves, and fruit, ranging from 0 kg/m^2 under bare soil to 22 kg/m^2 under corn, root mean square height (RMSH) ranging from 0.5 cm to 3.15 cm, correlation length (CL) ranging from 4 cm to 15 cm, soil moisture ranging from very dry (0.05 m^3/m^3) to very wet (0.5 m^3/m^3), and soil temperature ranging from 10°C to 28°C at station 126, as shown in Fig. 4. Fortnightly calibration of the PPMR and PLMR were carried out using cold (sky) and warm (blackbody) targets. Warm point calibrations were conducted weekly by positioning the PPMR/PLMR above a blackbody chamber equipped with microwave absorber and 16 temperature sensors. Cold point calibrations were carried out at midnight as per the tower schedule, with the PPMR and PLMR directed towards the sky. The calibration accuracy of both PPMR and PLMR was found to be less than 1.5 K. Weekly measurements of near-surface soil moisture (top 5 cm) were taken by a Hydra-probe Data Acquisition System (HDAS; [28]) throughout the quadrants to confirm the representativeness of the station. For a detailed description of the experiment and comprehensive information about the dataset, readers are referred to the publications

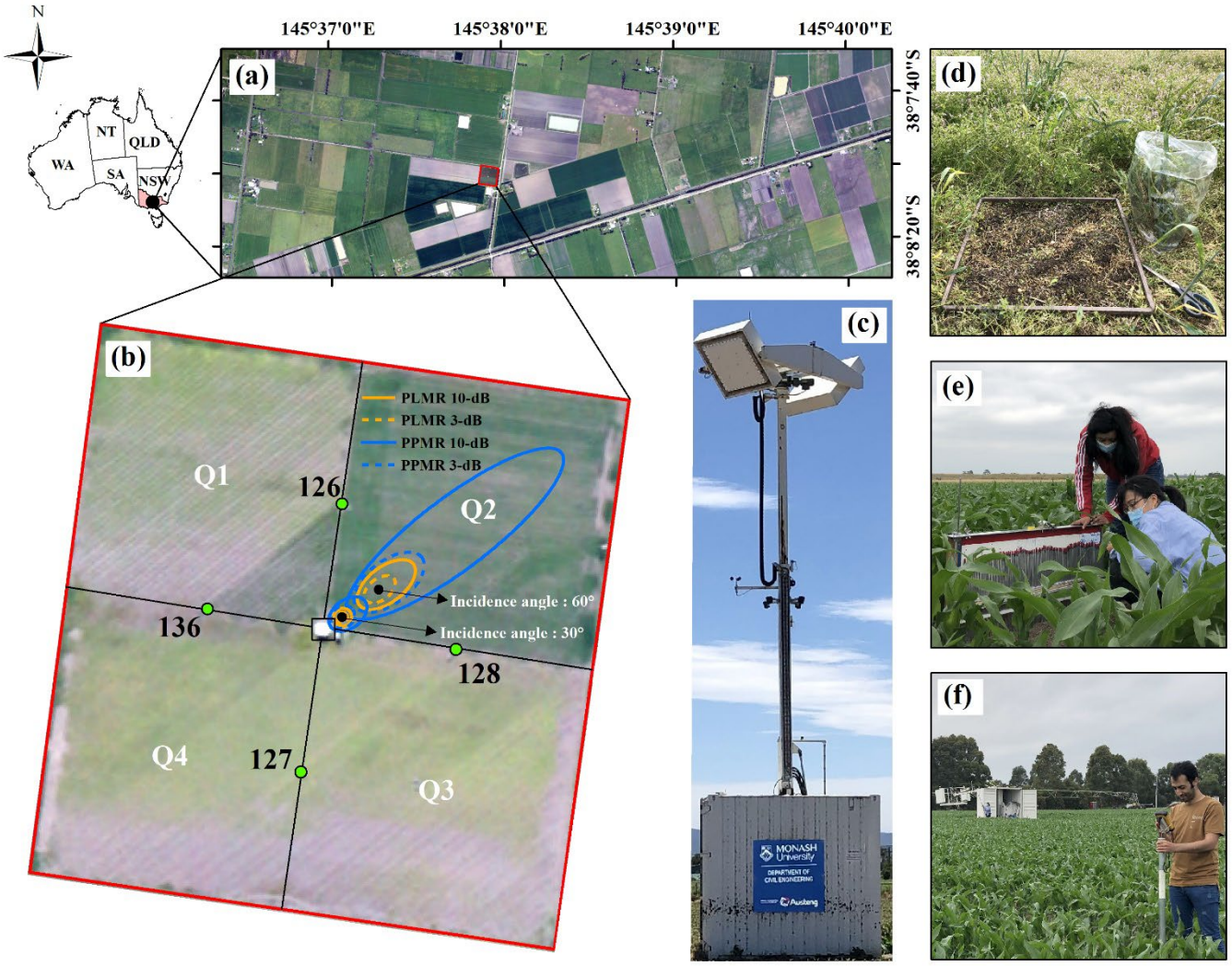

Fig. 1. Location map (a) of the experimental site (b) having a tower (c) at the center of a paddock at Cora Lynn, Victoria, Australia. The colored ovals represent the 3 and 10dB footprints of the microwave radiometers at incidence angles of 30° and 60°. The green dots on (b) represent the stations installed at the borders of the quadrants Q1 to Q4. The ancillary data of vegetation water content (d), surface roughness (e), and near-surface soil moisture at 0-5 cm using a Hydra-probe Data Acquisition System (HDAS, (f)), were collected weekly.

authored by Shen [11, 15] and the PRISM (P-band Radiometer Inferred Soil Moisture) project website (www.prism.monash.edu).

III. Methodology

Any object with a temperature higher than absolute zero (-273°C) emits thermal radiation, the intensity of which is directly proportional to its physical temperature. Radiometers measure the intensity of this thermal radiation from the soil in the form of TB, while models seek to simulate this radiation given the necessary input parameters. Under bare, smooth, homogeneous soils with uniform subsurface moisture and temperature profiles, the TB can be calculated using the well-known radiative transfer approximation (also known as the reciprocity approach or emissivity model; [29]) such that

$$TB_P = e_P T_s, \tag{1}$$

where T_s is the physical surface temperature (K), e_P is the emissivity of the body, and subscript P denotes either H or V polarization. Through Kirchhoff's reciprocity theory, the ground layer microwave emissivity of the target may be related (due to the reciprocal nature of the boundary conditions) to the fraction of the incident radiation reflected by a specular surface (r^*_P) according to

$$r^*_P = 1 - e_P. \tag{2}$$

Reflectivity for specular surfaces is determined by the Fresnel equations for H and V polarizations, respectively. These equations describe the behavior of electromagnetic waves at a smooth dielectric boundary according to [30]

$$r^*_H = \left| \frac{\cos(\theta) - \sqrt{\varepsilon_r - \sin^2(\theta)}}{\cos(\theta) + \sqrt{\varepsilon_r - \sin^2(\theta)}} \right|^2 \tag{3}$$

$$r^*_V = \left| \frac{\varepsilon_r \cdot \cos(\theta) - \sqrt{\varepsilon_r - \sin^2(\theta)}}{\varepsilon_r \cdot \cos(\theta) + \sqrt{\varepsilon_r - \sin^2(\theta)}} \right|^2, \tag{4}$$

where $\varepsilon_r = \varepsilon_r' + i\varepsilon_r''$ is the relative soil dielectric constant which includes real ($'$) and imaginary ($''$) parts, and θ is the incidence angle.

The emissivity model is a conventional passive microwave remote sensing model assuming a uniform soil moisture and temperature profile. However, when the temperature and moisture profile are not uniform and there is a variation near the surface, this model is not able to accurately capture the impact of the soil moisture and temperature variations [31], particularly for lower frequencies that have a response from deeper layers of the soil. Due to factors such as gravity, solar radiation, precipitation, and infiltration, soil moisture and soil temperature vary naturally with depth. When the subsurface moisture profile changes slowly in relation to the wavelength in the medium, the incoherent zero-order radiative transfer approximation [32] can be used to estimate the TB according to

$$TB_P = e_P \left\{ \int_{-\infty}^{0} T(z) \left(\frac{2\pi}{\lambda_0} \cdot \frac{\varepsilon_r''(z)}{2\sqrt{\varepsilon_r'(z)}} \right) exp\left[- \int_z^0 \alpha(z')dz' \right] dz \right\}, \tag{5}$$

where the expression in the round brackets represents the attenuation through the coefficient $\alpha(z)$, and the integral expression in curly brackets represents the effective temperature T_{eff} (K) of the soil medium. λ_0 is the free-space wavelength (m), and subscript z represent the depth (m).

From the incoherent model (Eq. 5), Burke and Paris [33], and Liu [34] developed multi-layer incoherent models based on first-order and incoherent solution approximations respectively. In the incoherent solution model, the reflections at the layer interfaces and the propagation of radiance through each layer are considered. In the first-order or zero-order approximations, either single reflections at interfaces are considered or reflections are ignored, respectively. Therefore, Eq. (5) is similar to Eq. (1), except that it more accurately represents the TB_P in terms of an "effective temperature" by considering the reflections at the different layers. This effective temperature, T_{eff}, is a weighted average of temperature at different depths, which may differ from the surface temperature, T_s. When data from regions with rapid changes in sub-surface moisture and temperature (either dry-down periods or regions with subsurface water tables) are analyzed, the incoherent model (Eq. 5) is also expected to become inaccurate, as it does not account for the coherent reflections anticipated from radiative transfer theory [35]. Therefore, the coherent models of Njoku and Kong [35] and Wilheit [36] were formulated in terms of continuous and discrete varying dielectric constant within the soil, such that

$$TB_P = \int_0^\infty T(z) W_P(z) dz, \tag{6}$$

$$TB_P = \int_0^\infty T(z) F_P(z) dz, \tag{7}$$

where $T(z)$ is the soil temperature at depth z, $\mathrm{W}_P(\mathrm{z})$ represents the relative contribution of each soil layer to the total radiation through a thermal weighting function, and $\mathrm{F}_P(\mathrm{z})$ represents the fraction of absorption. The calculation is strictly derived by solving Maxwell's field equations and is solely dependent on the frequency, polarization, incidence angle, and the dielectric constant profile of the soil. The theory behind these approaches utilizes electromagnetic fluctuations and electromagnetic wave propagation, as formulated by Stogryn [37]. Although both the Njoku and Wilheit models assume coherent radiation, the ways in which they calculate the observed intensities are entirely different, with the Wilheit model being conceptually and computationally simpler than the Njoku model. The formulation for deriving TB based on Eqs. (6) and (7) for a large number of horizontal layers, referred to as a stratified medium, was presented for the Njoku model in [35] and for the Wilheit

model in [36], for smooth and bare soil.

The five models - zero-order, first-order, incoherent solution, Njoku, and Wilheit - use the soil moisture and temperature profile as input to estimate the TB under bare smooth soil conditions. These are all stratified (i.e., multi-layer) models, and the profile depth and the layer thickness used herein were set to 1 m and 0.01 m (100 layers), respectively.

To consider roughness, the well-known hqn model developed by Wigneron [38] was utilized such that

$$r_P = \left[(1 - q_P)r^*{}_P + q_P r^*{}_Q\right] exp\left(-h_P cos^{n_P}(\theta)\right), \quad (8)$$

where r_P is the rough surface reflectivity (with $P = H$ and Q=V or $P = V$ and Q=H), h_P is the surface roughness parameter, q_P is the polarization mixing factor, and n_P is the angular dependence of the surface roughness. The h_P parameter is calculated using [38]

$$h_P = 1.3972 * \left(\frac{RMSH}{CL}\right)^{0.5879}, \quad (9)$$

where $RMSH$ and CL are the root mean square surface roughness height and correlation length parameters measured in the field. The parameter n_P was calibrated (based on q_P equal to zero for both L- and P- bands) from another period of the data and set to -0.50 (1.80) and -0.333 (0.415) at H (V) polarizations for L-band and P-band, respectively.

It is important to note that in this study, not all of the models employed account for multiple scattering within the vegetation layer. This assumption is considered reasonable, given the low frequency range utilized for soil moisture sensing. The effect of vegetation on the overall TB was considered using the tau-omega model developed by Mo [39] such that

$$TB_{TOV,P=}T_{eff}(1 - r_P)\Gamma_P + T_c(1 - \omega_P)(1 - \Gamma_P)(1 + r_P\Gamma_P) + TB_{AS,P}r_P\Gamma^2{}_P, \quad (10)$$

where T_c is the physical temperature of the vegetation canopy and assumed to be equal to surface temperature (T_s) at 6 AM [42, 43]. In all five of the models (three stratified incoherent and two stratified coherent) described above, an effective temperature T_{eff} is finally calculated, which can then be used in Eq. (10) to calculate the overall TB in response to rough vegetated surfaces. In the conventional tau-omega model of Eq. (10), a simple parametrization was developed by Wigneron [42] based on only T_s and the deep-soil temperature (T_{deep}) such that

$$T_{eff} = T_{deep} + \left(T_s - T_{deep}\right) * (sm / \omega_0)^{b_0}, \quad (11)$$

where ω_0 and b_0 are parameters that depend on specific soil characteristics (e.g., texture, structure, and density), which were set to 0.35 and 0.58 [43], respectively. Here, sm is the average soil moisture over the retrieval depths of L-band and P-band, considered to be 5 cm and 7 cm, respectively [10].

In Eq. (10), $TB_{AS,P}$ is the downward atmospheric contribution calculated to be to 5.3 K and 13.9 K at L-band and P-band respectively [44], while Γ_P is the vegetation transmissivity or vegetation attenuation factor, derived from the optical depth of the standing vegetation ($\tau_{veg,P}$) such that

$$\Gamma_P = \exp\left(-\frac{\tau_{veg,P}}{\cos\theta}\right). \quad (12)$$

Table 1. Overview of microwave emission models for soil moisture estimation. Abb: abbreviation, SM: soil moisture, ST: soil temperature, VE: vegetation, SRM: surface roughness model, DM: dielectric model, SC: scattering inside the soil, LoC: level of complexity, and Ref: reference. Multi means multi-layer with a minimum of 2 layers required; however, here it was set to 100 layers.

Model	Abb	Type	Number of layers			SRM	DM	SC	LoC	Ref
			SM	ST	VE					
tau-omega	TO	Incoherent	Single	Two	Single	hqn	MR GRMDM	Ignore	Very simple	[39]
Zero-order	IZ	Incoherent	Multi	Multi	Single	hqn	MR GRMDM	Ignore	Simple	[32]
First-order	IF	Incoherent	Multi	Multi	Single	hqn	MR GRMDM	Single	Moderate complex	[33]
Incoherent Solution	IS	Incoherent	Multi	Multi	Single	hqn	MR GRMDM	Multi	Complex	[34]
Njoku	NM	Coherent	Multi	Multi	Single	hqn	MR GRMDM	Ignore	Very complex	[35]
Wilheit	WM	Coherent	Multi	Multi	Single	hqn	MR GRMDM	Ignore	Moderate complex	[36]

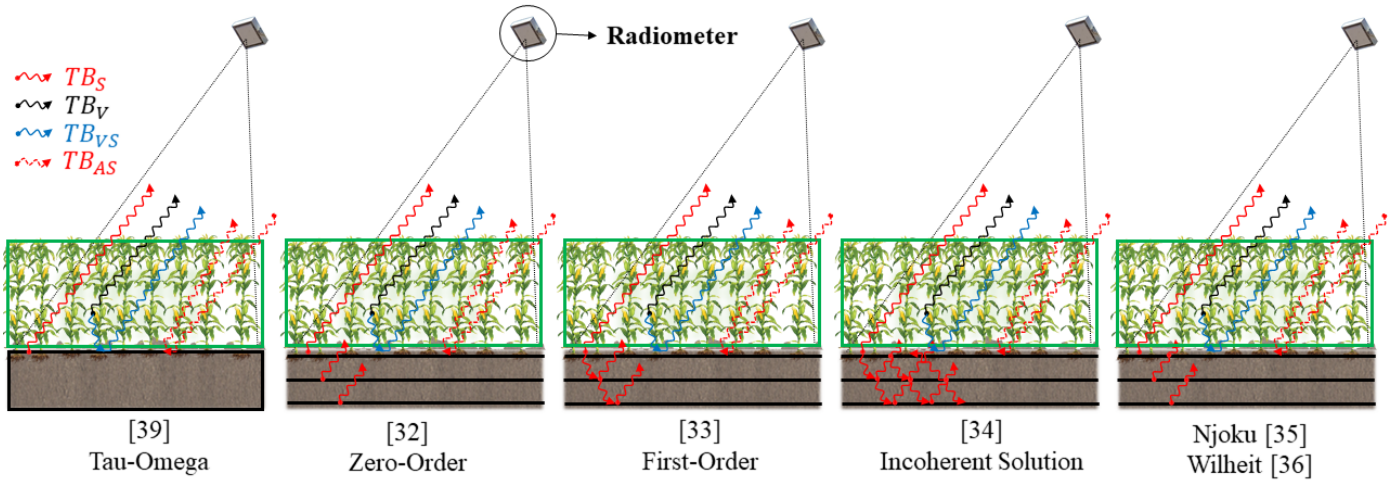

Fig. 2. Schematic of passive microwave emission models. The calculated brightness temperature (TB) for each model includes the sum of TB_S, TB_V, TB_{VS} and TB_{AS}. TB_S and TB_V represent emissions directly from soil and vegetation, respectively. TB_{VS} is the emission from the vegetation, reflected by the soil, while TB_{AS} is the downward emission from the sky reflected by the soil. Please note that the multilayer incoherent zero-order model and multilayer coherent Njoku and Wilheit models have similar schemes here; however, the former is different from the latter two models in terms of the physics law behind them. Additionally, Njoku and Wilheit models are entirely different in terms of formulation.

In the SMAP Single Channel Algorithm (SCA), VWC is used as a proxy to compute $\tau_{veg,P}$ according to [45]

$$\tau_{veg,P} = b \cdot \mathrm{VWC}, \tag{13}$$

where the b parameter is a proportionality value dependent on the vegetation type, structure, and observation frequency, and is typically taken as a constant over time for simplicity [45]. The b parameter was calibrated here under grass (0.11, 0.11), wheat (0.11, 0.099), and corn (0.094, 0.053) conditions for L-band and P-band, respectively. The scattering albedo (ω_p), defined as the ratio of the scattering to extinction coefficient ratios, was also calibrated here for grass (0.05, 0.05), wheat (0.05, 0.134), and corn (0.070, 0.086) conditions for L-band and P-band, respectively.

The aforementioned passive microwave models require the selection of an appropriate soil dielectric model to relate soil moisture to the dielectric constant. The multi-relaxation generalized refractive mixing dielectric model (MR GRMDM; [46]) was utilized for this purpose, as it accounts for the interfacial (Maxwell-Wagner) relaxation of water in the soil, which is important at P band [47]. Table 1 summarizes the key information, assumptions, advantages, and disadvantages of the two stratified coherent models of Njoku (hereafter NM) and Wilheit (WM), and four incoherent models including a conventional layer tau-omega model (TO), and the three multi-layer models of zero-order (IZ), first-order (IF), and incoherent solution (IS). A schematic of these models is shown in Fig. 2. In the following section, the results of these models are evaluated and compared for estimating TB.

IV. Results

A comprehensive assessment was conducted to evaluate the differences between estimated TB obtained from a range of coherent and incoherent models. The analysis used time series data of TB at L-band and P-band, profile soil moisture and soil temperature, VWC, and RMSH from a tower-based experiment, including data from three bare periods (Fig. 3) and periods with different vegetation types including grass, wheat, and corn (Fig. 4). To compare the six models quantitatively, values of TB at L- and P-band were calculated for each of the models using the *in situ* measurements of soil moisture, soil temperature, VWC, RMSH and CL shown in Fig. 3 and Fig. 4.

A. Model inter-comparison

The comparisons of the models at L-band and P-band frequencies can be seen in Fig. 3 for bare soil and in Fig. 4 for vegetated soil. Overall, the agreement among the six models was found to be good at both frequencies, closely following the observed TB. Based on the time series of estimated and observed TB in Fig. 3 and Fig. 4, the maximum differences between the models occurred during bare, grass, and wheat periods when the vegetation water content was low, and there was a high gradient of soil moisture near the surface, particularly during rainfall or irrigation events (one example is shown by the red circle in Fig. 4 (a1) and (a2)). The maximum differences were observed during the grass period (red circle in Fig. 4 (a1) and (a2)) between the coherent model (NM) and the incoherent zero-order model (IZ). The differences reached 16 K (18 K) at L-band and 26 K (42 K) at P-band H-polarization (V-polarization). This is consistent with previous research by Schmugge and Choudhury [27], who found that the maximum difference between these models was 21 K at L-band. The absolute differences between the models were calculated and plotted in Fig. 5. Generally, the agreement between the model's estimations is good for L-band, as can be seen from Fig. 5

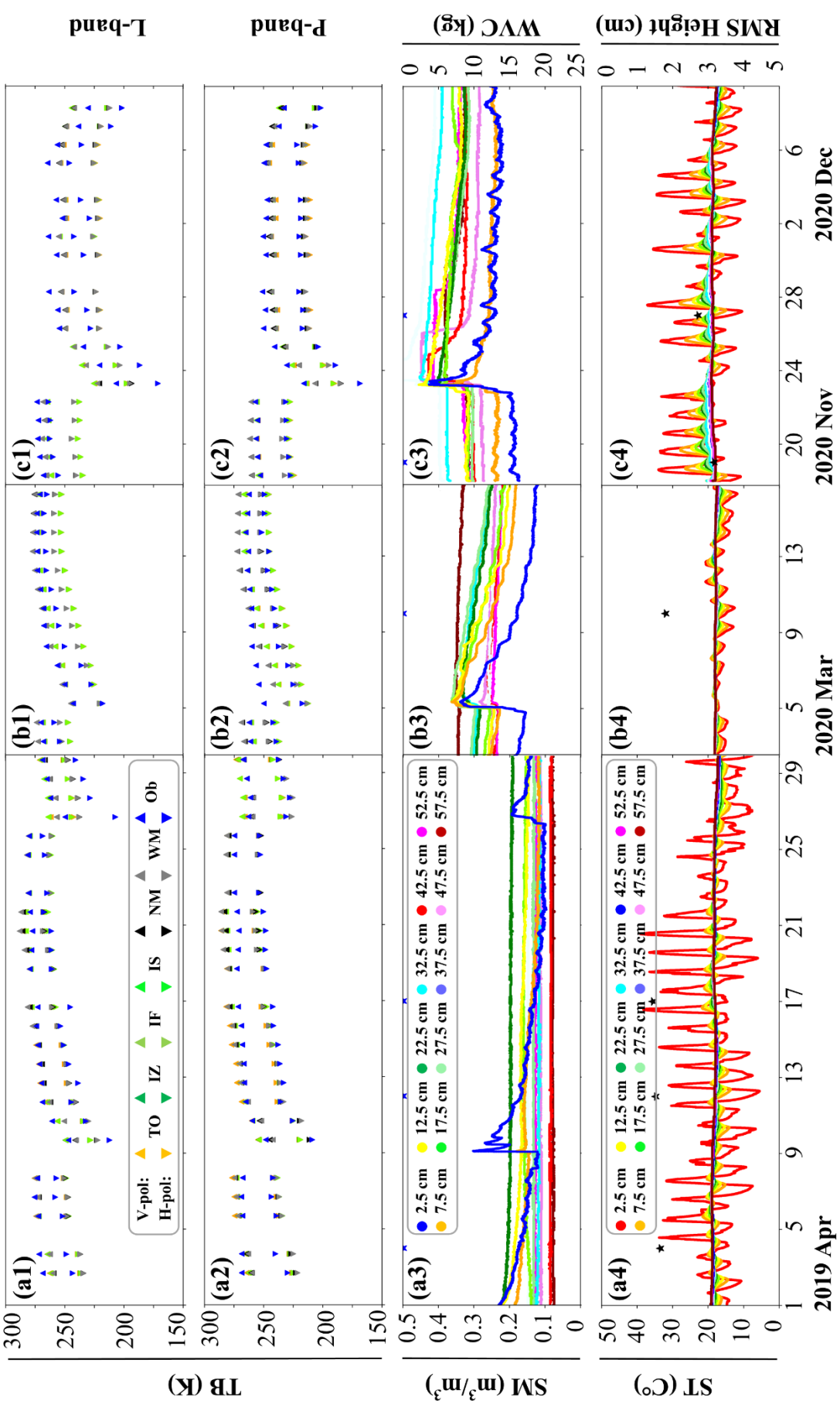

Fig. 3. The observed and estimated brightness temperature using passive microwave models during three bare soil periods: a) April 2019, b) March 2020, and c) November-December 2020, together with associated soil moisture and temperature observations at different soil depths. The blue stars in the soil moisture profile plots represents vegetation water content (VWC, in kg/m2) and the black stars in the soil temperature profile plots represents the root mean squared (RMS; in cm) roughness height. The indices 1, 2, 3, and 4 in each figure represent the L-band observation, P-band observation, soil moisture profile, and soil temperature profile, respectively. Note that TO, IZ, IF, IS, NM, and WM refer to the tau-omega, zero-order incoherent, first-order incoherent, incoherent solution, Njoku model, and Wilheit model, respectively.

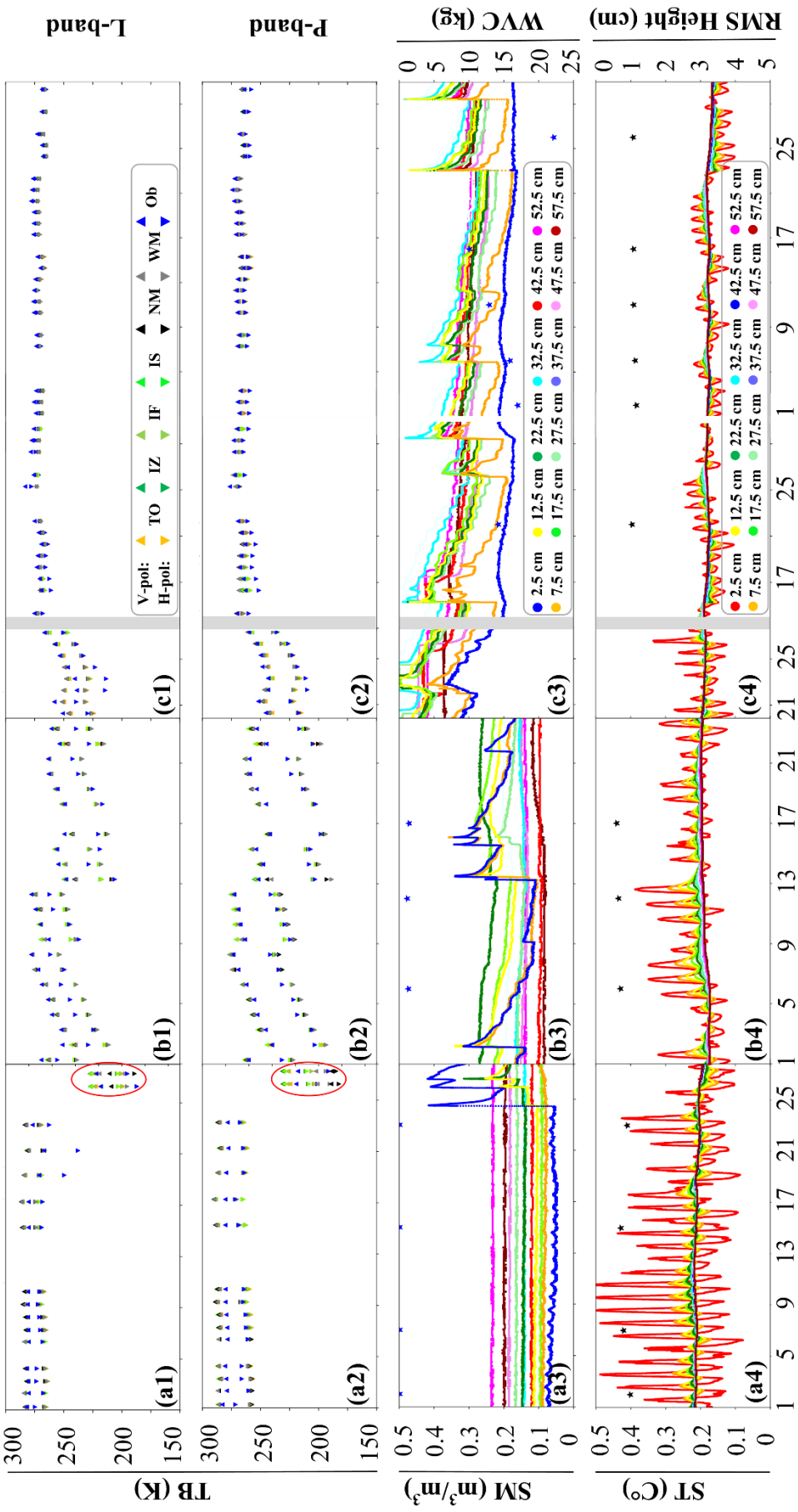

Fig. 4. As for Fig.3 but under three periods of vegetated soil: a) grass (March 2018), b) wheat (December 2018), and c) corn (December 2020 to March 2021). The blue stars in the soil moisture profile plots represents vegetation water content (VWC, in kg/m2) and the black stars in the soil temperature profile plots represents the root mean squared (RMS; in cm) roughness height. The indices 1, 2, 3, and 4 in each figure represent the L-band observation, P-band observation, soil moisture profile, and soil temperature profile, respectively. Note that TO, IZ, IF, IS, NM, and WM refer to the tau-omega, zero-order incoherent, first-order incoherent, incoherent solution, Njoku model, and Wilheit model, respectively. The gray area in the corn period is a 17-day gap where the tower was lowered due to unscheduled maintenance.

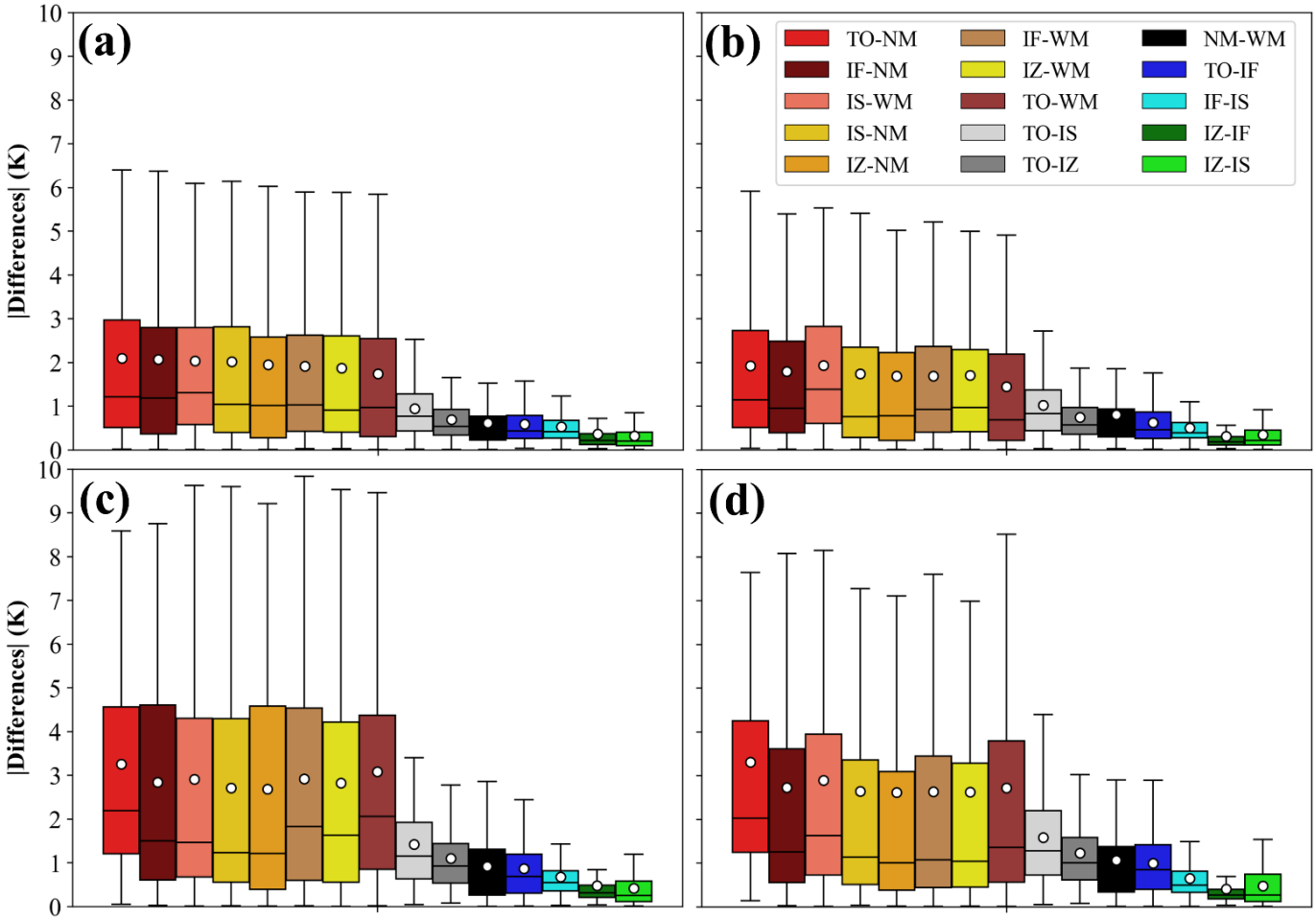

Fig. 5. The absolute difference between pairs of coherent models, incoherent models, and coherent and incoherent models, in terms of their estimation of brightness temperature using a) L-band (H-polarization), b) L-band (V-polarization), c) P-band (H-polarization), and d) P-band (V-polarization). Please note that TO, IZ, IF, IS, NM, and WM refer to the tau-omega, zero-order incoherent, first-order incoherent, incoherent solution, Njoku model, and Wilheit model, respectively. The white dot in each box represents the average value. The outlier was not shown in the plot due to its high values, suppressing the visualization of boxes.

(positively skewed distributions of the differences in the boxplot), with the maximum differences observed between the incoherent and coherent models, particularly between the TO and NM. These differences were approximately 2 K at L-band and 3 K at P-band, being slightly lower for V polarization compared with H polarization. At P-band, the minimum difference (the lowest average and median values) between coherent and incoherent models was observed for IZ and IS with NM. At L-band, this minimum difference was found between the IZ with NM and the TO with WM, as depicted in Fig. 5. When comparing the incoherent models, the minimum difference was found to be less than 0.5 K at both bands, occurring between the IZ model with the IF and IS models. The maximum value was found to be ~1 K between the TO and IS models. Additionally, the average difference between the coherent Njoku and Wilheit models at L-band and P-band was less than 1 K (Fig. 5).

B. Comparison of models with field measurements

To determine which model is more accurate, the estimated TB using each model was compared with the observed TB from the PLMR and PPMR radiometers at L-band and P-band, as shown in Fig. 6 and Table 2. The detailed error metrics including the root mean square error (RMSE), mean bias (Bias), unbiased RMSE (ubRMSE), and correlation coefficient (R) concerning the TB estimated by the models at L-band and P-band under different conditions (bare, grass, wheat, and corn), are listed in Table 2.

The models performed well at both bands, with strong positive correlations that were consistently high at both H and V polarization, ranging from 0.88 to 0.97. Generally, the RMSE at L-band was higher than at P-band as evident from Fig. 6 and Table 2. The results showed that the RMSE and ubRMSE were higher at L-band H-polarization (absolute RMSE around 10 K) compared to L-band V-polarization or P-band H or V-polarization, which had an RMSE of around 5 K (Table 2). As shown in Table 2, the coherent models were able to estimate TB at L-band H-polarization slightly more accurately compared to the incoherent models (RMSE 9.4 K compared to 10.6 K).

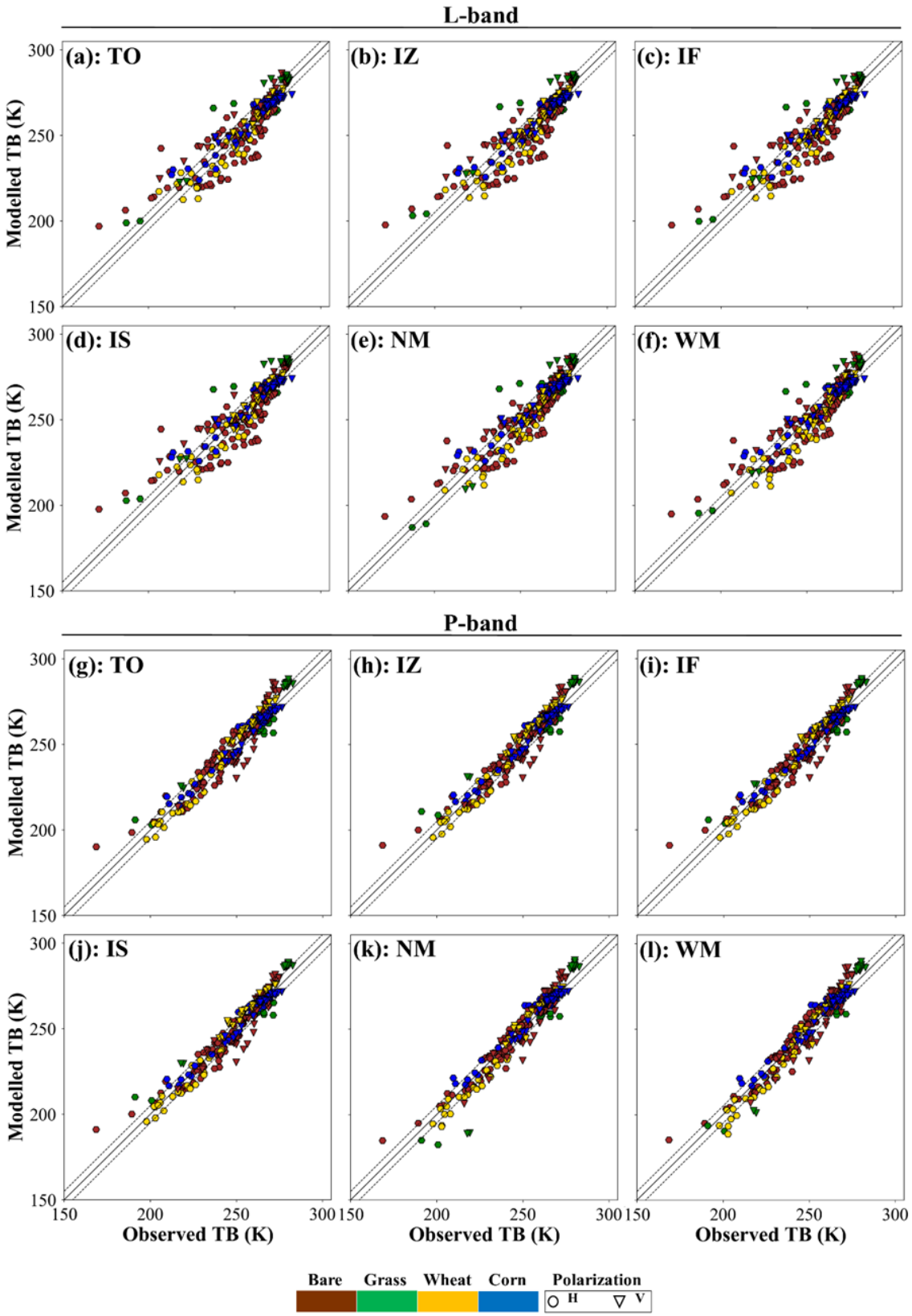

Fig. 6. Scatter plot of the observed and estimated brightness temperature at L-band and P-band using the following models: a and g) incoherent tau-omega (TO), b and h) incoherent zero-order (IZ), c and i) incoherent first-order (IF), d and j) incoherent solution (IS), e and k) Njoku model (NM), and f and l) Wilheit model (WM). The solid line is line 1:1 and the dash lines denote ± 5 K offset.

Table 2. Comparison of the coherent and incoherent models' TB estimations with tower-based measurements. RMSE, Bias, and ubRMSE are in kelvin (K). R represents the correlation coefficient, and N indicates the number of samples. The abbreviation of the models is interpreted as Fig. 5.

Model	RMSE (K)		Bias (K)		ubRMSE (K)		R		N
	H	V	H	V	H	V	H	V	
					L-band				
TO	10.64	5.42	2.39	1.14	10.37	5.3	0.88	0.92	141
IZ	10.61	5.33	2	0.73	10.42	5.28	0.88	0.93	141
IF	10.61	5.35	2.36	1.03	10.34	5.25	0.88	0.93	141
IS	10.57	5.34	2.01	0.74	10.38	5.29	0.88	0.92	141
NM	9.30	5.26	1.85	0.93	9.11	5.18	0.91	0.93	141
WM	9.46	5.31	1.95	1.07	9.26	5.2	0.91	0.93	141
					P-band				
TO	5.66	5.78	0.68	-0.80	5.62	5.72	0.97	0.94	141
IZ	5.52	5.54	0.10	-1.43	5.52	5.35	0.97	0.94	141
IF	5.33	5.37	0.57	-1.03	5.3	5.27	0.97	0.94	141
IS	5.33	5.44	0.14	-1.37	5.33	5.26	0.97	0.94	141
NM	5.40	6.27	0.19	-1.07	5.4	6.18	0.97	0.95	141
WM	5.51	5.89	0.18	-0.90	5.51	5.82	0.97	0.96	141

At P-band, both coherent and incoherent models performed similarly with an average RMSE around 5.5 K at H and V-polarization. The Bias values, representing the systematic error in the models, were positive at L-band (H-polarization, ~2 K), L-band (V-polarization, ~1 K), and P-band (H-polarization, ~0.3 K), while negative for P-band (V-polarization, ~-1 K).

At L-band, the differences between the model estimation and observations increased as the TB decreased. At the extremes, especially when the TB was very low (indicating high soil moisture), there was an overestimation of the brightness temperature for all models, particularly at L-band, where it is more noticeable. When TB was high, there was an overestimation of TB by the models under bare and grass periods at V-polarization, particularly at P-band, as can be seen in Fig. 6.

The performance of the models was compared under different soil conditions, as illustrated in Fig. 7. The difference between the two model approaches was more pronounced under bare soil at L-band H-polarization (with the coherent models being 3 K more accurate) compared to under vegetated soil (where the incoherent models were 1 K more accurate). Moreover, as vegetation increased, the differences between the two models decreased (as shown in Fig. 7). Furthermore, the RMSE decreased in the following order: corn < wheat < grass < bare soil. In fact, the higher the VWC, the lower the RMSE. This is especially obvious in L-band H-polarization (Fig. 7).

V. DISCUSSION

The intercomparison of the employed models showed that the maximum differences between the model's estimation of TB occurred during rapid drying out and particularly wetting up periods, such as heavy rainfall or irrigation. The reason could be due to the fact that heavy precipitation can lead to short-term surface wetting of vegetation and/or ponding of water on the ground's surface, which is not accounted for in the radiative transfer models and affects the radiometer's response and sensing depth due to changes in the dielectric constant of the scene. To avoid overestimation of soil moisture in the SMAP Level 2 passive soil moisture (L2SMP) product from such affects, a precipitation flag is included based on supplementary information about recent precipitation at the given location [48]. Additionally, maximum differences were observed between the coherent and incoherent model estimations at P-band. This can be attributed to the fact that this frequency has a longer wavelength and so responds to the moisture and temperature from a deeper layer of the soil, resulting in a greater sampling depth. The differences between the coherent and incoherent models was influenced by both the frequency being used and the steepness of the soil moisture gradient near the surface. The former was already shown in Fig. 5. The latter is shown in Fig. 8, in which the absolute difference between pairs

Table 3. Overview of average soil moisture at 5cm (SM, m^3/m^3), gradient of soil moisture at 0-5 to 5-10 cm (ΔSM, m^3/m^3), and vegetation water content (VWC, kg/m^2) under different land cover conditions. TO and NM are the tau-omega and Njoku models. H and V are polarization.

	Bare	**Grass**	**Wheat**	**Corn**
SM	0.18	0.1	0.19	0.21
ΔSM	0.031	0.055	0.014	0.05
VWC	0.1	0.08	1.33	13
TO-NM (L-band(H))	0.91	0.98	0.91	0.012
TO-NM (L-band(V))	0.81	0.99	0.95	-0.07
TO-NM (P-band(H))	0.86	0.97	0.71	0.41
TO-NM (P-band(V))	0.86	0.99	0.89	0.26

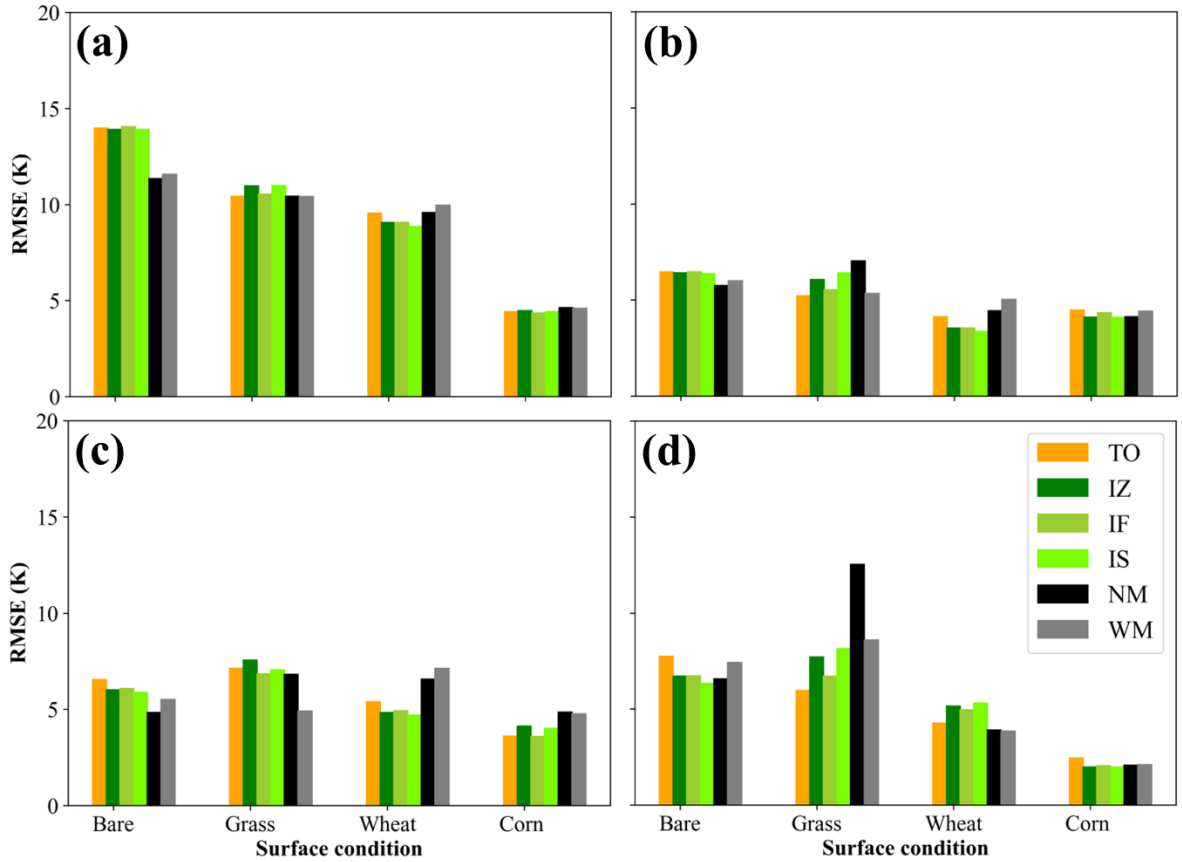

Fig. 7. RMSE between the observed and the estimated brightness temperature at a) L-band (H-polarization), b) L-band (V-polarization), c) P-band (H-polarization), and d) P-band (V-polarization) for the six different models tested on the four different surface conditions. The abbreviation of the models is interpreted as Fig. 5.

of coherent and incoherent models showed a strong correlation with the gradient of soil moisture at 0-5 cm to 5-10 cm. It was also shown that, except for differences between NM and WM, and IZ and IF models, the difference between the other pairs of incoherent models had a strong correlation with the gradient of soil temperature at 0-5 cm to 5-10 cm. The correlation between the absolute difference of the pairs of models with soil moisture and temperature at depth of 0-5 cm, VWC, RMSH, and CL was also calculated. The result showed no strong correlation between them, as shown in Fig. 8. It was also shown that vegetation water content can decrease the correlation between the absolute difference of the model's estimation with the absolute change of soil moisture at 0-5 cm and 5-10 cm as can be seen from Table 3. Table 3 clearly shows a strong correlation between the absolute difference of TO and NM estimation of TB at both L-band and P-band with absolute changes in soil moisture at 5 cm during bare, grass, and wheat periods. However, during the corn period, this correlation was weak at P-band (maximum 0.44 at H-polarization) and non-existent (~ 0) at L-band. For the corn period, both vegetation water content and soil moisture at the near-surface were higher compared to the other periods, as seen in Table 3. Accordingly, most of the L-band and P-band signals reaching the radiometers came from the vegetation and surface soil moisture in this situation. Therefore, even the simple incoherent single-layer model TO performed similarly to the very complex coherent multi-layer of NM, as seen in Fig. 7.

The estimation from all models was compared with the observed TB collected from the tower-based experiment. It was found that the RMSE between the estimated and observed TB at L-band H-polarization was higher than that at V-polarization or P-band (H-polarization or V-polarization). The higher RMSE at L-band may be attributed to the greater sensitivity of the H-polarization to surface roughness or soil moisture [48, 49], or by misrepresentation of soil moisture at shallow depths. The microwave emission depth depends on both the soil moisture condition and the sensor configuration (e.g., frequency, incidence angle) though the effective sensing depth of soil moisture at L-band and P-band is generally considered as 2-5 cm and 7 cm, respectively [51]–[56]. While the surface is drying, the upper layer is drier than the subsurface, resulting in higher TB at L-band H-polarization. However, all the models use the average soil moisture below the surface, which is typically wetter compared to the surface due to drying processes, and therefore results in a lower modeled TB.

Lower sensitivity of V-polarization compared to H-polarization is also evident from Fig. 6, as the dynamic range of TB at H-polarization is higher than at V-polarization. The lower sensitivity of V-polarization to soil moisture and surface roughness has been confirmed in many studies [47]. Therefore, a lower RMSE at V-polarization can provide a very promising

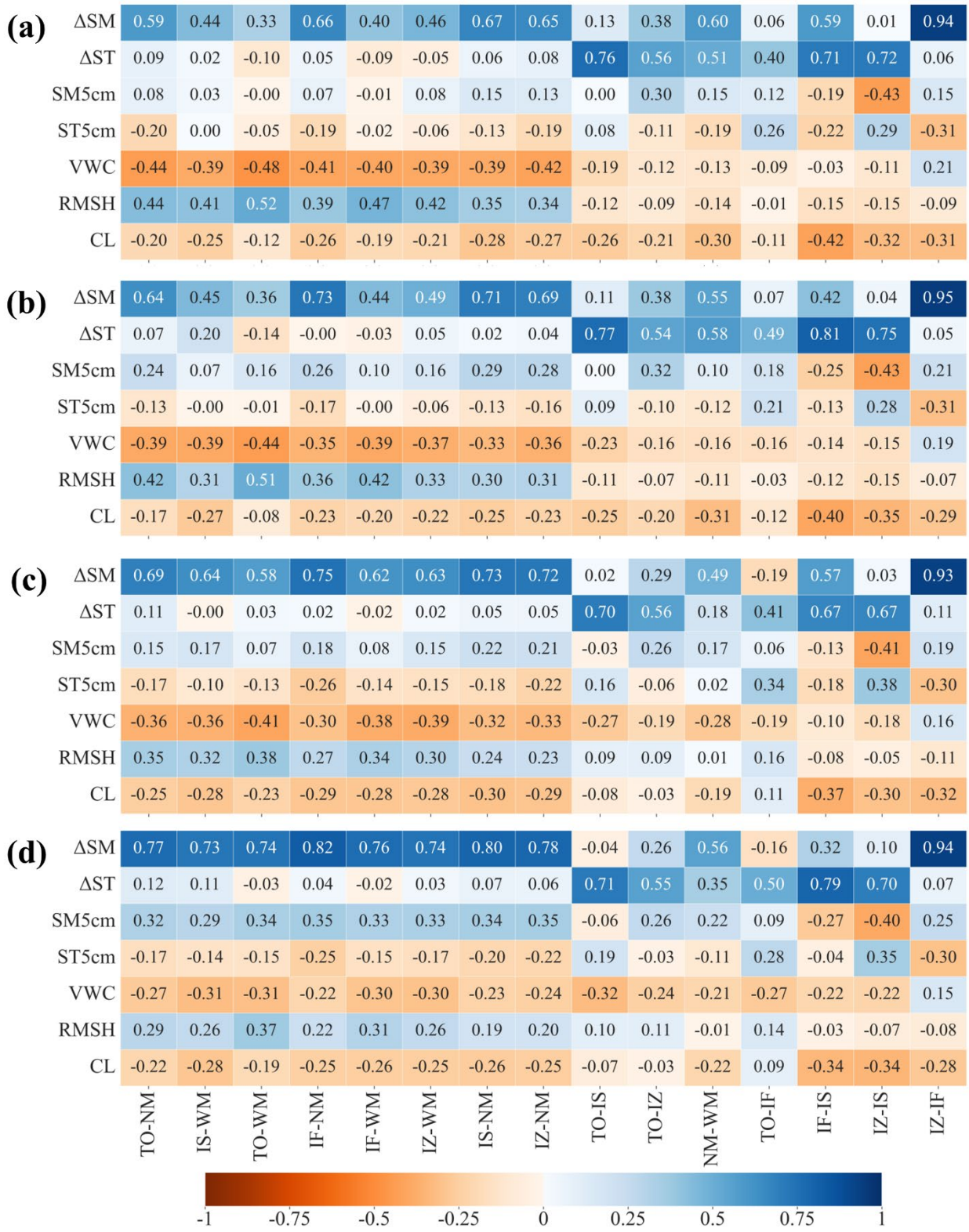

Fig. 8. Correlation coefficients (R) between the absolute difference between pairs of the models with soil moisture at depth of 0-5 cm (SM5cm), soil temperature at depth of 0-5 cm (ST5cm), differences between soil moisture and temperature at depth of 0-5 cm and 5-10 cm (ΔSM and ΔSM respectively), vegetation water content (VWC), root mean square height (RMSH), and correlation length (CL) at a) L-band (H-polarization), b) L-band (V-polarization), c) P-band (H-polarization), and d) L-band (V-polarization). The abbreviation of the models is interpreted as Fig. 5.

way to estimate soil temperature, as it is weakly dependent on surface roughness and soil moisture.

The model's estimation of TB was also analyzed under different land cover conditions. The lowest RMSE was found under corn canopy. The lower RMSE of the models under higher VWC may be due to two reasons. First, vegetation can attenuate and normalize emissions from the soil. Therefore, by having accurate information of VWC a lower RMSE is achieved. Second, converse to vegetated soil, under bare soil, the process of drying and wetting happens more rapidly, leading to a steeper gradient of soil moisture in the shallow layers. This steep gradient of soil moisture makes it challenging to obtain accurate measurements of soil moisture, leading to higher RMSE values.

Both coherent and incoherent models have a certain level of complexity. However, incoherent models are generally simpler, and therefore can be calculated faster, but their accuracy was slightly lower compared to coherent models. Some models are simpler than others, regardless of whether they are coherent or incoherent. For instance, the Wilheit coherent model is simpler than the Njoku model, and the conventional incoherent tau-omega model is simpler than the multi-layer zero-order model. The conventional tau-omega model only requires average soil moisture and effective temperature as input, but the incoherent multi-layer model requires input of both soil moisture and soil temperature profiles. If the intention is to obtain information about the distribution of moisture or temperature within the soil, using a conventional tau-omega model may not be the most suitable choice. Therefore, it is necessary to trade the importance of accuracy against model simplicity when making a model selection. Accordingly, a radiative transfer model that is more sophisticated may provide more precise results, but it may also be too resource-intensive for practical application or require inputs that are not readily available. This paper provides valuable insights into the performance of passive microwave emission models, emphasizing the need for further refinement and exploration in this field.

VI. Conclusion

Several forms of coherent and incoherent models were compared for estimating TB, including two models that were stratified and coherent, three stratified models that were incoherent and based on approximations of scattering, including zero-order, first-order, and incoherent solutions, and the conventional single-layer tau-omega model. The study used simultaneous soil moisture and temperature profile measurements under different land cover conditions, including three periods with bare soil, one with grass, one with wheat, and one with corn, along with measurements of TB at L-band and P-band frequencies, as well as weekly measurements of vegetation water content and surface roughness from a tower-based experiment conducted at Cora Lynn, Victoria, Australia.

A comparison between the coherent and incoherent models revealed that, overall, the agreement among the six models was good at both L-band and P-band frequencies, with close alignment to observed TB. The maximum differences were between pairs of coherent and incoherent models with the average difference being 3 K at P-band and 2 K at L-band. The difference between the coherent and incoherent models were a function of frequency and steepness of soil moisture at shallow layers. Maximum differences between model estimates occurred during rapid drying and wetting periods, particularly following heavy rainfall or irrigation, emphasizing the impact of short-term surface wetting on radiometer response and the fact that this scenario is not accounted for in the radiative transfer models.

Model predictions of TB were compared with observations from radiometers at L-band and P-band, revealing strong positive correlations ranging from 0.88 to 0.97. The calculated RMSE between the observed and estimated TB from the models indicated that the coherent models could more accurately estimate TB by 3 K under bare soil, while the incoherent models could more accurately estimate TB by 1 K under vegetated soil. Differences between model approaches decreased with increasing vegetation, and RMSE decreased with higher vegetation water content.

In general, the coherent models tended to perform slightly better than the incoherent models, however based on these results, the additional complexity of a coherent model does not seem to be justified by its potential improvement in performance. This research contributes valuable insights into the performance of passive microwave emission models, shedding light on their strengths and limitations under different environmental conditions. The findings provide a foundation for future research aimed at refining and optimizing these models for practical applications in soil moisture estimation.

ACKNOWLEDGMENT

This work was supported by the Australian Research Council through the Towards P-Band Soil Moisture Sensing from Space Project under Discovery Grant DP170102373, and Linkage, Infrastructure, Equipment and Facility Grants LE0453434 and LE150100047. The authors thank Pascal Mater and Kiri Mason for their help with maintenance of the experimental equipment and site. Thanks also to Mr. Wayne Tymensen for kindly providing the land for the experiment site.

REFERENCES

[1] T. Oki and S. Kanae, 'Global Hydrological Cycles and World Water Resources', *Science*, vol. 313, no. 5790, pp. 1068–1072, Aug. 2006, doi: 10.1126/science.1128845.

[2] J.-S. Cai *et al.*, 'Importance of variability in initial soil moisture and rainfalls on slope stability', *J. Hydrol.*, vol. 571, pp. 265–278, Apr. 2019, doi: 10.1016/j.jhydrol.2019.01.046.

[3] A. Berg and J. Sheffield, 'Climate Change and Drought: the Soil Moisture Perspective', *Curr. Clim. Change Rep.*, vol. 4, no. 2, pp. 180–191, Jun. 2018, doi: 10.1007/s40641-018-0095-0.

[4] L. Zhao, M. Yebra, A. I. J. M. van Dijk, G. J. Cary, and D. Hughes, 'Controlled field experiment clarifies the influence of soil moisture on litter moisture content',

Agric. For. Meteorol., vol. 314, p. 108782, Mar. 2022, doi: 10.1016/j.agrformet.2021.108782.

[5] S.-B. Kim, L. Tsang, J. T. Johnson, S. Huang, J. J. van Zyl, and E. G. Njoku, 'Soil Moisture Retrieval Using Time-Series Radar Observations Over Bare Surfaces', *IEEE Trans. Geosci. Remote Sens.*, vol. 50, no. 5, pp. 1853–1863, May 2012, doi: 10.1109/TGRS.2011.2169454.

[6] H. McNairn *et al.*, 'The Soil Moisture Active Passive Validation Experiment 2012 (SMAPVEX12): Prelaunch Calibration and Validation of the SMAP Soil Moisture Algorithms', *IEEE Trans. Geosci. Remote Sens.*, vol. 53, no. 5, pp. 2784–2801, May 2015, doi: 10.1109/TGRS.2014.2364913.

[7] E. G. Njoku and D. Entekhabi, 'Passive microwave remote sensing of soil moisture', *J. Hydrol.*, vol. 184, no. 1–2, pp. 101–129, 1996.

[8] Y. H. Kerr *et al.*, 'The SMOS Mission: New Tool for Monitoring Key Elements ofthe Global Water Cycle', *Proc. IEEE*, vol. 98, no. 5, pp. 666–687, May 2010, doi: 10.1109/JPROC.2010.2043032.

[9] D. Entekhabi, S. Yueh, and G. De Lannoy, 'SMAP handbook', 2014.

[10] X. Shen *et al.*, 'Soil Moisture Retrieval Depth of P- and L-Band Radiometry: Predictions and Observations', *IEEE Trans. Geosci. Remote Sens.*, pp. 1–9, 2020, doi: 10.1109/TGRS.2020.3026384.

[11] X. Shen *et al.*, 'Impact of random and periodic surface roughness on P- and L-band radiometry', *Remote Sens. Environ.*, vol. 269, p. 112825, Feb. 2022, doi: 10.1016/j.rse.2021.112825.

[12] H. Ma *et al.*, 'An assessment of L-band surface soil moisture products from SMOS and SMAP in the tropical areas', *Remote Sens. Environ.*, vol. 284, p. 113344, 2023.

[13] Svoboda, P., Raimanová, I., Duffková, R., Fučík, P., Kurešová, G., and Haberle, J., 'The effects of irrigation on root density profiles of potato, celery, and wheat', p. 911.1Kb, 2020, doi: 10.15159/AR.20.035.

[14] N. Ye *et al.*, 'Toward P-Band Passive Microwave Sensing of Soil Moisture', *IEEE Geosci. Remote Sens. Lett.*, pp. 1–5, 2020, doi: 10.1109/LGRS.2020.2976204.

[15] F. Brakhasi *et al.*, 'Towards soil moisture profile estimation in the root zone using L- and P-band radiometer observations: A coherent modelling approach', *Sci. Remote Sens.*, vol. 7, p. 100079, Jun. 2023, doi: 10.1016/j.srs.2023.100079.

[16] X. Shen *et al.*, 'Evaluation of the tau-omega model over bare and wheat-covered flat and periodic soil surfaces at P- and L-band', *Remote Sens. Environ.*, vol. 273, p. 112960, May 2022, doi: 10.1016/j.rse.2022.112960.

[17] A. G. Konings, D. Entekhabi, S. K. Chan, and E. G. Njoku, 'Effect of Radiative Transfer Uncertainty on L-Band Radiometric Soil Moisture Retrieval', *IEEE Trans. Geosci. Remote Sens.*, vol. 49, no. 7, pp. 2686–2698, Jul. 2011, doi: 10.1109/TGRS.2011.2105495.

[18] F. T. Ulaby and D. G. Long, *Microwave radar and radiometric remote sensing*. Ann Arbor: The University of Michigan Press, 2014.

[19] J. Muñoz-Sabater *et al.*, 'Assimilation of SMOS brightness temperatures in the ECMWF Integrated Forecasting System', *Q. J. R. Meteorol. Soc.*, vol. 145, no. 723, pp. 2524–2548, Jul. 2019, doi: 10.1002/qj.3577.

[20] G. J. De Lannoy and R. H. Reichle, 'Assimilation of SMOS brightness temperatures or soil moisture retrievals into a land surface model', *Hydrol. Earth Syst. Sci.*, vol. 20, no. 12, pp. 4895–4911, 2016.

[21] J. F. Galantowicz, D. Entekhabi, and E. G. Njoku, 'Tests of sequential data assimilation for retrieving profile soil moisture and temperature from observed L-band radiobrightness', *IEEE Trans. Geosci. Remote Sens.*, vol. 37, no. 4, pp. 1860–1870, 1999.

[22] R. H. Reichle, D. Entekhabi, and D. B. McLaughlin, 'Downscaling of radio brightness measurements for soil moisture estimation: A four-dimensional variational data assimilation approach', *Water Resour. Res.*, vol. 37, no. 9, pp. 2353–2364, Sep. 2001, doi: 10.1029/2001WR000475.

[23] G. J. De Lannoy, R. H. Reichle, and V. R. Pauwels, 'Global calibration of the GEOS-5 L-band microwave radiative transfer model over nonfrozen land using SMOS observations', *J. Hydrometeorol.*, vol. 14, no. 3, pp. 765–785, 2013.

[24] P. De Rosnay *et al.*, 'AMMA Land Surface Model Intercomparison Experiment coupled to the Community Microwave Emission Model: ALMIP-MEM', *J. Geophys. Res. Atmospheres*, vol. 114, no. D5, p. 2008JD010724, Mar. 2009, doi: 10.1029/2008JD010724.

[25] G. J. De Lannoy, R. H. Reichle, and J. A. Vrugt, 'Uncertainty quantification of GEOS-5 L-band radiative transfer model parameters using Bayesian inference and SMOS observations', *Remote Sens. Environ.*, vol. 148, pp. 146–157, 2014.

[26] J. Qiu, J. Dong, W. T. Crow, X. Zhang, R. H. Reichle, and G. J. De Lannoy, 'The benefit of brightness temperature assimilation for the SMAP Level-4 surface and root-zone soil moisture analysis', *Hydrol. Earth Syst. Sci.*, vol. 25, no. 3, pp. 1569–1586, 2021.

[27] T. J. Schmugge and B. J. Choudhury, 'A comparison of radiative transfer models for predicting the microwave emission from soils', *Radio Sci.*, vol. 16, no. 5, pp. 927–938, Sep. 1981, doi: 10.1029/RS016i005p00927.

[28] O. Merlin, J. P. Walker, R. Panciera, R. Young, J. D. Kalma, and E. J. Kim, 'Calibration of a soil moisture sensor in heterogeneous terrain', in *MODSIM 2007 International Congress on Modelling and Simulation. Modelling and Simulation Society of Australia and New Zealand*, 2007, pp. 2604–2610.

[29] W. Peake, 'Interaction of electromagnetic waves with some natural surfaces', *IRE Trans. Antennas Propag.*, vol. 7, no. 5, pp. 324–329, 1959.

[30] T. Schmugge, 'Measurements of surface soil moisture and temperature', in *Remote sensing of biosphere functioning*, New York, NY.: Springer, 1990, pp. 31–63.

[31] E. G. Njoku, J. P. Schieldge, and A. B. Kahle, 'Joint microwave and infrared studies for soil moisture determination', 1980.

[32] F. T. Ulaby, R. K. Moore, and A. K. Fung, 'Microwave remote sensing: Active and passive. Volume 3-From theory to applications', 1986.

[33] W. J. Burke and J. F. Paris, 'A radiative transfer model for microwave emissions from bare agricultural soils', 1975.

[34] P.-W. Liu, R. D. De Roo, A. W. England, and J. Judge, 'Impact of Moisture Distribution Within the Sensing Depth on L- and C-Band Emission in Sandy Soils', *IEEE J. Sel. Top. Appl. Earth Obs. Remote Sens.*, vol. 6, no. 2, pp. 887–899, Apr. 2013, doi: 10.1109/JSTARS.2012.2213239.

[35] E. G. Njoku and J.-A. Kong, 'Theory for passive microwave remote sensing of near-surface soil moisture', *J. Geophys. Res.*, vol. 82, no. 20, pp. 3108–3118, Jul. 1977, doi: 10.1029/JB082i020p03108.

[36] T. T. Wilheit, 'Radiative Transfer in a Plane Stratified Dielectric', *IEEE Trans. Geosci. Electron.*, vol. 16, no. 2, pp. 138–143, Apr. 1978, doi: 10.1109/TGE.1978.294577.

[37] A. Stogryn, 'The Brightness Temperature of a Vertically Structured Medium', *Radio Sci.*, vol. 5, no. 12, pp. 1397–1406, Dec. 1970, doi: 10.1029/RS005i012p01397.

[38] J.-P. Wigneron, L. Laguerre, and Y. H. Kerr, 'A simple parameterization of the L-band microwave emission from rough agricultural soils', *IEEE Trans. Geosci. Remote Sens.*, vol. 39, no. 8, pp. 1697–1707, Aug. 2001, doi: 10.1109/36.942548.

[39] T. Mo, B. J. Choudhury, T. J. Schmugge, J. R. Wang, and T. J. Jackson, 'A model for microwave emission from vegetation-covered fields', *J. Geophys. Res.*, vol. 87, no. C13, p. 11229, 1982, doi: 10.1029/JC087iC13p11229.

[40] E. Fagerlund, B. Kleman, L. Sellin, and H. Svensson, 'Physical studies of nature by thermal mapping', *Earth-Sci. Rev.*, vol. 6, no. 3, pp. 169–180, 1970.

[41] T. Jackson and J. Kimball, 'SMAP Mission Science Issues Associated with Overpass Time', *SMAP Sci. Doc.*, no. 003, 2009.

[42] J.-P. Wigneron, A. Chanzy, P. de Rosnay, C. Rudiger, and J.-C. Calvet, 'Estimating the Effective Soil Temperature at L-Band as a Function of Soil Properties', *IEEE Trans. Geosci. Remote Sens.*, vol. 46, no. 3, pp. 797–807, Mar. 2008, doi: 10.1109/TGRS.2007.914806.

[43] S. Lv, J. Wen, Y. Zeng, H. Tian, and Z. Su, 'An improved two-layer algorithm for estimating effective soil temperature in microwave radiometry using in situ temperature and soil moisture measurements', *Remote Sens. Environ.*, vol. 152, pp. 356–363, Sep. 2014, doi: 10.1016/j.rse.2014.07.007.

[44] ITU, 'International telecommunication union recommendation: Radio noise', 2015.

[45] T. J. Jackson and T. J. Schmugge, 'Vegetation effects on the microwave emission of soils', *Remote Sens. Environ.*, vol. 36, no. 3, pp. 203–212, Jun. 1991, doi: 10.1016/0034-4257(91)90057-D.

[46] Mironov, P. P. Bobrov, and S. V. Fomin, 'Multirelaxation Generalized Refractive Mixing Dielectric Model of Moist Soils', *IEEE Geosci. Remote Sens. Lett.*, vol. 10, no. 3, pp. 603–606, May 2013, doi: 10.1109/LGRS.2012.2215574.

[47] L. Zhang, Q. Meng, D. Hu, Y. Zhang, S. Yao, and X. Chen, 'Comparison of different soil dielectric models for microwave soil moisture retrievals', *Int. J. Remote Sens.*, vol. 41, no. 8, pp. 3054–3069, Apr. 2020, doi: 10.1080/01431161.2019.1698077.

[48] M. Neelam *et al.*, 'Evaluation of GEOS precipitation flagging for SMAP soil moisture retrieval accuracy', *J. Hydrometeorol.*, vol. 22, no. 5, pp. 1317–1332, 2021.

[49] J. Zeng, K.-S. Chen, H. Bi, T. Zhao, and X. Yang, 'A comprehensive analysis of rough soil surface scattering and emission predicted by AIEM with comparison to numerical simulations and experimental measurements', *IEEE Trans. Geosci. Remote Sens.*, vol. 55, no. 3, pp. 1696–1708, 2016.

[50] S. Hong, 'Surface roughness and polarization ratio in microwave remote sensing', *Int. J. Remote Sens.*, vol. 31, no. 10, pp. 2709–2716, May 2010, doi: 10.1080/01431161003627855.

[51] M.-J. Escorihuela, A. Chanzy, J.-P. Wigneron, and Y. H. Kerr, 'Effective soil moisture sampling depth of L-band radiometry: A case study', *Remote Sens. Environ.*, vol. 114, no. 5, pp. 995–1001, 2010.

[52] Y. H. Kerr, P. Waldteufel, J.-P. Wigneron, J. Martinuzzi, J. Font, and M. Berger, 'Soil moisture retrieval from space: The Soil Moisture and Ocean Salinity (SMOS) mission', *IEEE Trans. Geosci. Remote Sens.*, vol. 39, no. 8, pp. 1729–1735, 2001.

[53] A. Chanzy *et al.*, 'Airborne microwave radiometry on a semi-arid area during HAPEX-Sahel', *J. Hydrol.*, vol. 188, pp. 285–309, 1997.

[54] T. Schmugge and T. J. Jackson, 'Mapping surface soil moisture with microwave radiometers', *Meteorol. Atmospheric Phys.*, vol. 54, no. 1–4, pp. 213–223, 1994.

[55] J. Wang, 'Microwave Emission from Smooth Bare Fields and Soil Moisture Sampling Depth', *IEEE Trans. Geosci. Remote Sens.*, vol. GE-25, no. 5, pp. 616–622, Sep. 1987, doi: 10.1109/TGRS.1987.289840.

[56] X. Shen *et al.*, 'Soil Moisture Retrieval Depth of P- and L-Band Radiometry: Predictions and Observations', *IEEE Trans. Geosci. Remote Sens.*, vol. 59, no. 8, pp. 6814–6822, Aug. 2021, doi: 10.1109/TGRS.2020.3026384.